Excellent capture of N_2O functioning at RT and the lower pressure by utilizing NaCaA-85 zeolite

S. Hiraki,[1] H. Baba,[1] I. Kobayashi,[1] A. Oda,[1,2] T. Ohkubo,[1] Y. Ikemoto[3], T. Moriwaki[3] and Y. Kuroda[1]

[1]Department of Chemistry, Graduate School of Natural Science and Technology, Okayama University, 3-1-1 Tsushima-naka, Kita-ku, Okayama 700-8530, Japan.

[2]Department of Materials Chemistry, Graduate School of Engineering, Nagoya University, Furo-cho, Chikusa-ku, Nagoya 464-8603, Japan.

[3]Japan Synchrotron Radiation Research Institute (JASRI), 1-1-1, Kouto, Sayo-cho, Sayo-gun, Hyogo 679-5198, Japan.

Supplementary Information

1. In connection with the interaction operated in the present system: the data obtained in the NaSrA-85–N_2O system and their comparison with those in the NaCaA-85–N_2O system.

Ionic radius of Ca^{2+} is smaller than that of Sr^{2+}: **Tab. S1b**. By comparing the adsorption properties of the Sr^{2+} ion exchanged A-type zeolite sample with those of the Ca^{2+} ion exchanged A-type zeolite sample, we can get the information on the nature of interaction between M^{2+} (Ca^{2+} or Sr^{2+}) exchanged in zeolite with lattice O_L (lattice oxygen) atom, and also on the adsorption behaviour for N_2O in both systems. To satisfy these purposes, we carried out the comparison of data with the help of the additional experiments: measurements of adsorption isotherms, mid-IR and far-IR in the NaSrA-85–N_2O system. On the basis of these experiments, we were aiming at getting the information on the following points:

a. The vibration modes of both ν_1 and ν_3 were expected to be influenced by the strength, as well as the types, of the interaction between exchanged M^{n+}-ion and an N_2O molecule. The important effect caused by the electronic field strength emanating from the Ca^{2+}-ion exchanged sample is expected to bring about the appearance of the absorption band of N_2O at higher wave-number in comparison with case of the exchanged Sr^{2+}-ion. In the case of strong adsorption found in this work, the increases in the adsorption amounts may be expected to take place especially in the initial adsorption region.

b. The electronic field strength due to the exchanged cation also directly affects the vibration mode between exchanged cation and lattice oxygen atom (O_L): M^{2+}–O_L which is observable in the far-IR region.

1-1 Adsorption

It is expected that the larger charge density of the exchanged Ca^{2+}-ion strongly interacted with an adsorbed N_2O molecule, as well as negatively charged lattice oxygen atom or atoms, i.e. $[(O_L)_n]$, compared to the case of the exchanged Sr^{2+}-ion. On the basis of the results in the text, it seems that there is no specific chemical bonding formation between the exchanged ion and an N_2O molecule. From the viewpoints of the adsorption features, the exchanged Ca^{2+}-ion with radius of 100 pm induces larger induced dipole moment for the adsorbed N_2O molecules in zeolites, in comparison with the case of the Sr^{2+}-ion with ionic radius of 118 pm exchanged sample. First of all, we measured the adsorption isotherms of the NaSrA-85 sample for N_2O and depicted in **Fig. S4** against the equilibrium pressure. The adsorbed amounts of 8.33, 20.8, 32.9, 63.5, 74 and 93 $cm^3\ g^{-1}$ at equilibrium pressure of 0.02, 0.1, 0.3, 4, 10 and 37.3 Torr, respectively. These values are compared with the data for NaCaA-85: 9.25, 21.3, 30.1, 56.1, 70 and 94 $cm^3\ g^{-1}$ at equilibrium pressure of 0.02, 0.1, 0.3, 4, 10 and 37.3 Torr, respectively. To easily understand the difference in the adsorbed amounts in both samples, the data for both samples in the lower pressure regions are also given in the same figures as **Fig. S5**. These data indicate that the adsorbed amounts of the NaSrA-85 sample are slightly lower in the lower equilibrium pressure region, whereas the values for the NaSrA-85 sample are larger than those for the

NaCaA-85 sample from the medium pressures. On the basis of these data, it is not too far from the truth that the difference in the lower pressure region is caused by the difference in the electric field strength operated in the interaction between M^{2+} and the interacted N_2O molecule, although it is not to be denied that the additional factor may be associated with the possibility that the distance between the Ca^{2+} ions is appropriate to form the pinned structure of N_2O with two kinds of metal ions. The increase in the adsorbed amount observed for NaSrA-85 sample in the higher pressure region may be related to the contribution of polarizability of cation exchanged: **Tab. S1b**. Actually, some authors have reported that Ba-ion exchanged zeolites exhibits excellent adsorption nature for an N_2O and molecule and also a CO_2 molecule.[1,2]

1-2 Mid IR

In the lower pressure region, the ν_1 bans caused by the adsorbed N_2O molecule on the exchanged metal ions (M^{2+}–N_2O species) was observed at the value of higher wave-number from the value of gas phase (1285 cm^{-1}), which was observed at 1302 cm^{-1} for the NaCaA-85 sample and is also higher than that observed for the NaSrA-85-N_2O system, i.e. 1296 cm^{-1}: **Fig. S6**. As for ν_3 band, NaCaA-85 gives band at 2276 cm^{-1} and the band at 2254 cm^{-1} for NaSrA-85, where the ν_3 mode of a gaseous molecule appears at 2223 cm^{-1}. For easy understanding these changes, the wave-numbers in both modes are also plotted as a function of equilibrium pressure in **Fig. S7**. The observation of changes in the shifts from gaseous phase in both cases may be associated with the fact that the position of cations are suitable for the formation of pinned structure of N_2O. The large changes in the wave-number on adsorption of N_2O toward higher values are observed both ν_1 and ν_3 modes, especially, in the lower equilibrium pressure region from 0 to 0.1 Torr which supports to the formation of the pinned adsorption structure through the respective cations exchanged in different sites. In this region, two kinds of exchanged Ca^{2+} ions cause "induced dipole moment" in an adsorbed N_2O molecule, in both ν_1 (N-O) and ν_3 (N-N) bands simultaneously, through the interactions with Ca^{2+} ions positioned in both sides of adsorbed N_2O molecule. In this adsorption model, it is reasonably explained by considering that the dipole moments were simultaneously induce by two types of the exchanged M^{2+} ions, resulting in the shifts towards the higher sides in both modes: ν_1 and ν_3. On the other hand, the changing behaviour of both modes in this region is vague in NaSrA-85 sample, although the adsorbed amounts are almost same as that for NaCaA-85 sample. This may be attributable to the presence of some kinds of adsorption modes may be existing in the NaSrA-85 sample, i.e., the effect of polarizability of the cations, and also the exchanged Ca^{2+} ions occupied more suitable positions for forming the pinned N_2O species as compared with the case of the NaSrA-85 sample.

2. The discussion on the bonding nature of the M-O_L mode based on far-IR data

The spectra observed in the far-IR region are related to the change in the vibrational modes

between M^{2+} and O_L before and after adsorption of N_2O. Therefore, the far-IR study on zeolite system make it possible to obtain directly the important information on the interaction between the exchanged cation and the lattice oxygen atom (O_L). Actually, we carried out *in situ* measurement in the far-IR region for N_2O adsorption on the NaCaA-85 sample and succeeded in getting information on the Ca^{2+}–O_L mode as shown in the text and also in **Fig. S8**. Here, we have also performed the Far-IR measurement for the system of NaSrA-85 before and after N_2O adsorption. However, there is a problem to obtain the information on the Sr^{2+}–O_L mode directly from the measured spectrum: **Fig. S9a**. This is because the observed bands is difficult to assign this mode correctly from the spectrum. To circumvent this point, we took advantage of getting the difference spectrum before and after N_2O adsorption on the NaSrA-85 sample: **Fig. S9b**. The bonding nature will be discussed by comparison with the difference spectra obtained in both samples.

In this discussion, we adopted a rough approximation composed of the simple model, i.e., (M^{2+}–O_L) pair where $M^{2+} = Ca^{2+}$ and Sr^{2+}.

$$\nu \propto \sqrt{\frac{k}{\mu}} \qquad (1)$$

where $\boldsymbol{k}$ means force constant and $\boldsymbol{\mu}$ reduced mass.

First of all, we assumed that the force constant between (M^{2+}–O_L) pair remains constant in both systems. On this assumption, we evaluated by adopting the wave-number of vibration of 275 cm^{-1} between M^{2+} and O_L found in experiment for NaCaA-85. In that case, the wave-number for the M^{2+}–O_L pair in NaSrA-85 sample is evaluated to be 253 cm^{-1} by way of the simple model described just above. This value is too large in comparison the value obtained by actual value, 208 cm^{-1} as shown in **Fig. S8b**. This difference are attributable to the difference in force constants in respective systems. On the basis of this consideration, we can evaluate the difference between two systems: (Ca^{2+}–O_L) pair and (Sr^{2+}–O_L) pair in the present samples. The relative magnitude in force constants results in the following data; the value for the former is 1.5 times larger than that for the latter. From the remarks obtained in the experiments related to the NaSrA-85 and NaCaA-85 systems, one general point becomes clear; the dominant interaction operated in these systems is caused by the electrostatic field emanated from the exchanged cations. Needless to say, this difference may also include another structural factor; the exchanged cations occupied more suitable positions for the formation of bridged N_2O species.

3. A comparison of adsorption behaviour of NaCaA-85 for N_2O with that for other gases

The most striking aspect of the present result was that the adsorption specificity was only seen in a CaA-type zeolite with the higher exchanging level: NaCaA-85. It is expected that the specific adsorption model proposed in this work endows the NaCaA-85 sample with the discrimination of the

N_2O molecule against other simple molecules, such as diatomic molecules of N_2 and O_2, as well as CH_4 with spherical structure in shape, although these molecules have almost similar kinetic diameters: **Tab. S1a**. Such idea leads us to examine the adsorption selectivity for simple molecules: N_2, O_2 and CH_4. Shown in **Fig. S11a** are the adsorption isotherms of the NaCaA-85 sample against N_2, O_2 and CH_4, respectively. As anticipated, the N_2 and O_2 molecules are scarcely adsorbed on this sample in the equilibrium pressure region from 0 to 100 Torr. CH_4 was also only slightly adsorbed on this sample. This slight increase in the amount may be interpreted by considering the contribution of dispersion force, resulting from the difference in the values of polarizability among three kinds of molecules. Anyway, these adsorption data shown in the figure justify further our proposed model in the specific adsorption of N_2O onto the NaCaA-85 sample, as well as pave a new way as the separation material for application.□

Thus far, little attention has been drawn to the researches on N_2O adsorption/separation by use of various types of materials, in comparison with the experiments on CO_2 adsorption/separation. To the best of our knowledge, there are little researches utilizing the efficient N_2O adsorption materials. Hence, we could hardly find the data focused on the N_2O selectivity. Under such circumstance, we tried to evaluate the separation selectivity (equilibrium selectivity factor the value of $\alpha = (V_{N2O}/V_{CH4})$ for methane, as well as $\alpha = (V_{N2O}/V_{N2})$ for dinitrogen, $\alpha = (V_{N2O}/V_{O2})$ for dioxygen, where V_{N2O} and V_{CH4}, V_{N2} and V_{O2} are the equilibrium molar adsorption amounts of N_2O, CH_4, N_2 and O_2 at given equilibrium pressures. These values were evaluated from the corresponding respective single component isotherms at given equilibrium pressures and given in **Fig. S11b**: [$\alpha = (V_{N2O}/V_{CH4})$] as well as another one [$\alpha = (V_{N2O}/V_{N2})$]. However, the data on the system (N_2O and O_2) were difficult to calculate, because of the adsorbed amounts of O_2 on this sample (NaCaA-85 sample) being too small.

For comparison, we examine our data with those evaluated on the basis of comparable single adsorption data for the selectivity of CO_2/CH_4 which was reported by some researches, e.g., M. Palomino et al.[3] This fact indicates possible usages of the NaCaA-85 sample for selective adsorption/separation for N_2O/CH_4, as well as N_2O/N_2 or O_2. In addition, this indication also supports that our system shows prominent separation of N_2O from the mixture gases including N_2, O_2 and CH_4

As the further information, taking into account the fact that the value of V_{CO2} are larger than the values of V_{N2O} in the present system (see Fig. S2), it may be said that the adsorption selectivity of this sample for CO_2 over CH_4 may deserve special mention.

Finally, the data mentioned in this work indicate the importance of the present system for N_2O adsorption/separation phenomena which may be useful in the application process. I hope that this work will attract wide attention of researchers working in these fields. The development of adsorbents working efficiently for N_2O has been becoming an enduring challenge in recent years as discussed in COP28 held in Dubai in 2023.

4. Experimental details

4.1 Materials: The substitution of Si^{4+} in zeolite by Al^{3+} results in excess negative charges in the lattice, which are balanced by compensating cations that occupy specific sites. In the present case, the Na form of A-type zeolite (NaA; $[Na_{12}(H_2O)_{27}]_8[Al_{12}Si_{12}O_{48}]_8$: Si/Al =1) purchased from Sigma-Aldrich Co., was used as the starting sample for obtaining the Ca^{2+}-ion- or Sr^{2+}-ion-exchanged sample: (NaCaA, NaSrA). The ion-exchanging operation was carried out at 373 K for 4 h in aqueous solutions of $Ca(NO_3)_2$, as well as $Sr(NO_3)_2$, *ca.* 3 g of zeolite was dispersed into an aqueous solution of 0. 5 mol/L, 200 mL. This operation was repeated five or seven times to obtain the samples with the desired exchanged capacities. The obtained samples were centrifuged and washed thoroughly with distilled water, followed by drying *in vacuo* at RT. The metal contents in the samples were determined by inductively coupled plasma (ICP) analysis (Varian Vista-Pro CCD Simultaneous ICP-ODS: Seiko Instruments & Varian Instruments). The obtained samples were evaluated to have 85% ion-exchange capacities (called NaCaA-85 and NaSrA-85, respectively). Here, the ion-exchange level (%) was estimated by assuming that one divalent cation is exchanged for two monovalent Na ions. We also used the purchased sample (CaA) from Sigma-aldrich Co. as the reference standard sample. The ion exchange capacity of this sample is evaluated by our group to be 78%: abbreviated as CaA-78, where the last number indicates the ion exchange capacity. The following gases used in this work were purchased from GL Sciences Co. (Tokyo, JP): N_2O (99.5%), CH_4 (99.9%), N_2 (99.99%) and O_2 (99.9%).

4.2 Adsorption measurements: The adsorption isotherms of N_2O at 298 K were obtained volumetrically using a volumetric adsorption apparatus equipped with an MKS Baratron pressure sensor (type 390). The 1st adsorption measurement was performed at 298 K on respective samples treated at 723 K for 4 h under a reduced pressure of 1.3 mPa. After the first run, the samples were re-evacuated at 298 K for 4 h, followed by measurement of the second adsorption at 298 K. The difference in adsorbed amounts between 1st and 2nd adsorption isotherms indicates the existence of the strongly adsorbed species.

4.3 **(1)** ***Mid-IR spectra***: The IR spectra were recorded at RT on a Digilab FTS-4000 spectrophotometer with a mercury cadmium telluride (MCT) detector kept at the temperature of liquid N_2 (accumulation: 256 scans; nominal resolution of 2 cm^{-1}) in the region between 4000–800 cm^{-1} in the transmission mode at RT for the self-supported sample by using an *in situ* cell developed by our group. The powdered sample was pressed into a pellet of 10 mm in diameter, and thus prepared disk was loaded into an IR cell that is capable of *in situ* treatment under a reduced pressure of 1 mPa and also consecutive in situ gas dosage.[4] Prior to IR measurements, the sample was first evacuated at 723 K to produce the standard state of the sample, followed by cooling to RT in the *in situ* condition. In addition, to get into the information on the adsorbed states of N_2O under various equilibrium pressure regions from lower pressure of 0.1 Torr to medium pressure of *ca.* 5 Torr at RT. All spectra

given in figures are depicted as the difference spectra between respective spectra for the N_2O adsorbed under various equilibrium-pressures and a spectrum of gas phase only.

(2) ***Far-IR spectra***: In this work, we focused on the exchanged cation-framework vibrational modes being observable in the far-IR region and their shifts upon N_2O adsorption. There are some difficulties in obtaining the detailed information from the far-IR region based on the experimental viewpoint. We designed *in situ* cell which was available in vacuum and the *in situ* condition after evacuating at higher temperatures and also in consecutive gas dosages. Furthermore, to obtain the information with high sensitivity on the role of exchanged Ca^{2+} or Sr^{2+} ions for the specific N_2O adsorption observed in the NaCaA-85 as well as NaSrA-85 samples at RT, we measured far-IR spectra in this system by taking advantage of SOR light, which is bright compared with the conventional IR sources, leading to the precise detection of the definitive change in the cation-vibrational modes of the Ca^{2+}- or Sr^{2+}-zeolite lattice vibrations through the adsorption of N_2O at RT. The measurements in the far-IR region were performed by using the BL43-IR beam line at the SPring-8 facility (Harima, Hyogo Prefecture, Japan) and using the spectrometer Bruker IFS 120 HR (Detector TGS). The Mylar 3.5 μm beam splitter was used in this work, as it was suitable for the spectral regions required here.[5]

4.4 Computational methodology (calculation method)

(1) Calculation conditions. DFT cluster calculations were conducted using the Gaussian 09 program. All calculations were performed at the B3LYP/6-31G(d,p) level with the SCF convergence criterion of 10^{-8} au.

(2) Models.

(2-1). Dual Ca^{2+} site: The DFT cluster model of the local environment of a type-A zeolite, i.e., $Al_4Si_{11}O_{16}H_{28}$ geometry that includes the 4MR, 6MR and 8MR sites, was adopted on the basis of the crystallographic data. To meet the charge compensation requirement from the zeolite framework, two Ca ions were placed at the 6MR and 8MR position as counter cations. Geometrical optimization was performed on the coordinates of all atoms except for the framework Si atoms, through which we obtained the cluster model that represents the dual Ca^{2+} sites located at the 6MR and 8MR positions: [^{8MR}Ca, ^{6MR}Ca]-$Al_4Si_{11}O_{16}H_{28}$. This model is the same one used in our preceding work.[6]

(2-2). N_2O adsorbed on the dual Ca^{2+} site: An N_2O molecule was placed close to a dual Ca^{2+} site, and the coordinates of all atoms except for the framework Si atoms were optimized. In this optimization process, two local minima were found. One is the N_2O molecule adsorbed on both two Ca ions in a bridge style: [^{8MR}Ca(N_2O)^{6MR}Ca]-$Al_4Si_{11}O_{16}H_{28}$. Other models were the N_2O molecule adsorbed on only the Ca ion sitting at the 8MR position and also at the 6MR position, respectively: [^{8MR}Ca(N_2O), ^{6MR}Ca]-$Al_4Si_{11}O_{16}H_{28}$ and at the 6MR position [^{8MR}Ca, ^{6MR}Ca(N_2O)]-$Al_4Si_{11}O_{16}H_{28}$ cluster models. All the geometries are given in **Fig. S-10**.

(2-3). Vibrational frequency calculations. To reproduce the mid- and far-IR spectra upon the process of N_2O adsorption on the [^{8MR}Ca, ^{6MR}Ca]-$Al_4Si_{11}O_{16}H_{28}$ cluster model, vibrational frequency calculations were performed on the [^{8MR}Ca, ^{6MR}Ca]-$Al_4Si_{11}O_{16}H_{28}$, [^{8MR}Ca(N_2O)^{6MR}Ca]-$Al_4Si_{11}O_{16}H_{28}$, [^{8MR}Ca(N_2O), ^{6MR}Ca]-$Al_4Si_{11}O_{16}H_{28}$, and [^{8MR}Ca, ^{6MR}Ca(N_2O)]-$Al_4Si_{11}O_{16}H_{28}$ cluster models. In these calculations, terminated H atoms were kept frozen.

(2-4). Adsorption energy calculations. The pre-optimized geometries were used. Then, dispersion correction was included by single-point energy calculations at B3LYP/6-31G(d,p) with empirical dispersion GD3.[7] Adsorption energy was defined as the following equation: $E_{ads} = E$[site-N_2O] - [site] - E[N_2O], where E[site-N_2O], E[site] and E[N_2O] mean the energy of the N_2O-adsorbed site, the site with no N_2O adsorption and free N_2O molecule. E_{ads} for the respective adsorption modes were summarized in **Table given below**.

In order to obtain the additional justification of the adsorption model, we tried to use these data. Contrary to expectations, the most stable adsorption mechanism was (^{8MR}CaN_2O, ^{6MR}Ca); adsorption at the 8MR site was stable in comparison with that for the bridge adsorption mechanism (^{8MR}CaN_2O^{6MR}Ca) by *ca.* 1 kJ/mol. However, we must insist here that this energy difference is within the error of the DFT calculation method. Therefore, we consider that the energy differences shown in **Table** are not sufficient to discuss the superiority of each adsorption site for N_2O.

Table DFT-predicted E_{ads} for the respective adsorption mechanisms.

Adsorption mode	E_{ads} (kJ/mol)
^{8MR}Ca(N_2O)^{6MR}Ca	**-84.2**
^{8MR}Ca(N_2O), ^{6MR}Ca	**-85.4**
^{8MR}Ca, ^{6MR}Ca(N_2O)	**-77.9**

Fig. S1. S. Hiraki et al.,

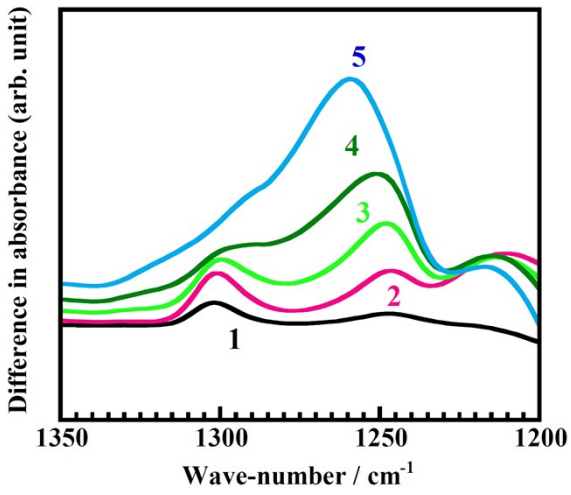

Fig. S1: Difference spectra in the symmetric ν_1 fundamental vibration region of the adsorbed N_2O molecules on the NaCaA-85 sample at increasing equilibrium pressures from 0 to 4.9 Torr. All spectra are the difference between respective states and spectrum of the spectrum evacuated at 723 K. The NaCaA-85 sample equilibrated with N_2O at (1) 0.04 Torr, (2) 0.10 Torr, (3) 0.70 Torr, (4) 1.4 Torr and (4) 4.9 Torr, respectively. All measurements were performed at RT.

Fig. SI-2. S. Hiraki et al.,

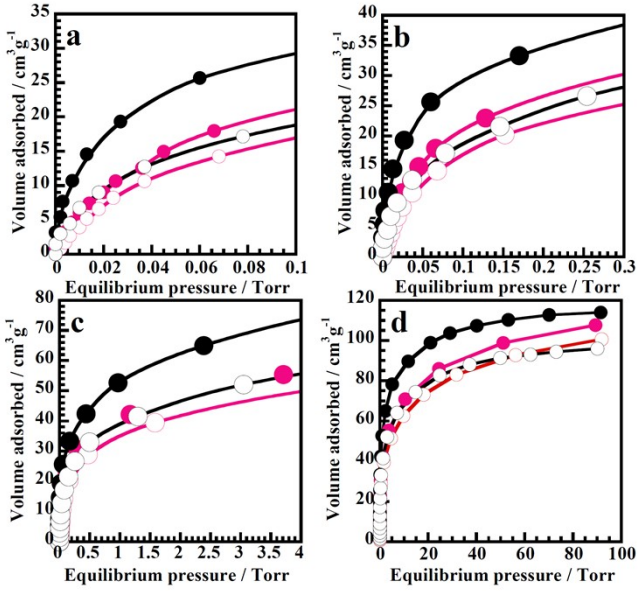

Fig. S2: The 1st (solid marks) and 2nd (open marks) adsorption isotherms of both CO_2 (**Black**) and N_2O (**Red**) at 298 K on the NaCaA-85 sample: pressure region between (a) 0–0.1 Torr; (b) 0–0.3 Torr; (c) 0–4 Torr; (d) 0–100 Torr.

Fig. S3. S. Hiraki et al.,

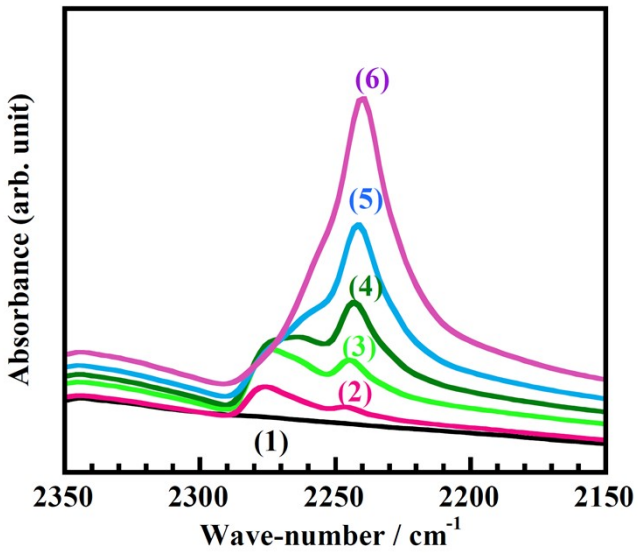

Fig. S3: The MID-IR absorption spectra of the adsorbed N_2O molecules on the NaCaA-85 sample at increasing equilibrium pressures from 0 to 4.9 Torr in the the asymmetric ν_3 fundamental vibration: the N-N(-O) mode. The NaCaA-85 sample was first (1) evacuated at 723 K; followed by equilibrating with N_2O at (2) 0.04 Torr; (3) 0.10 Torr; (4) 0.70 Torr; (5) 1.4 Torr; (6) 4.9 Torr, respectively. All measurements were performed at RT.

With reference to the ν_3 (N-N stretching) band region of N_2O, the major band first appeared at 2276 cm^{-1} accompanying by the weak band at 2245 cm^{-1} in the initial adsorption stage. With further increase in the equilibrium pressure to 4.9 Torr, the first band gradually shifted toward lower wave-number side and the band at 2245 cm^{-1} increases its intensity. Taking into accounts of the equilibriums pressure, the former band is characteristic for this sample and assigned to the adsorbed N_2O molecule peculiarly formed on the present sample. The latter band is attributed to the physisorbed N_2O species. Although the comparable IR data are sparse, the reported IR data as far as we know are as follows; 2241 cm^{-1} for BaFAU, 2237 cm^{-1} for CaFAU, 2234 cm^{-1} for MgFAU, 2238 cm^{-1} for BaCHA, 2236 cm^{-1} for CaCHA, 2230 cm^{-1} for CaFAU(Y), 2240 cm^{-1} for MgMOR: where FAU, CHA and MOR mean the types of zeolites: Faujasite, Chabazite and Mordenite type zeolites, respectively.[1,8] The 2276 cm^{-1} band observed in our case is the highest value thus far reported, indicating that the characteristic adsorption takes place in our system, i.e. strongly adsorbed N_2O species is formed in this system in harmony with the isotherm data (Fig.1).

Fig. S4. S. Hiraki et al.,

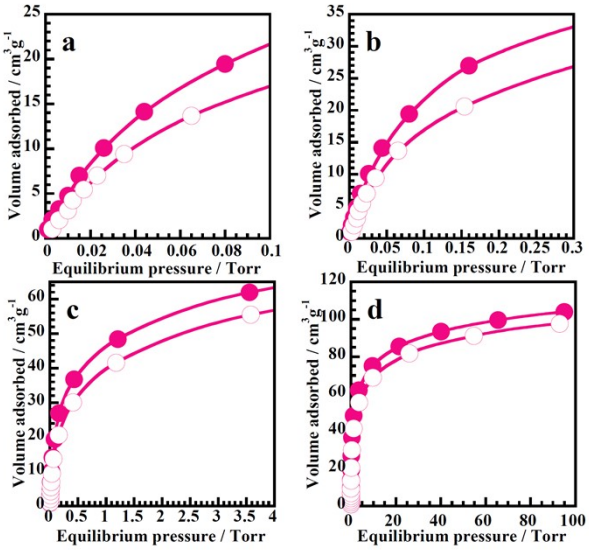

Fig. S4: The 1st (solid marks) and 2nd (open marks) adsorption isotherms of N_2O at 298 K on the NaSrA-85 sample: pressure region between (a) 0–0.1 Torr; (b) 0–0.3 Torr; (c) 0–4 Torr; (d) 0–100 Torr.

Fig. S5. S. Hiraki et al.,

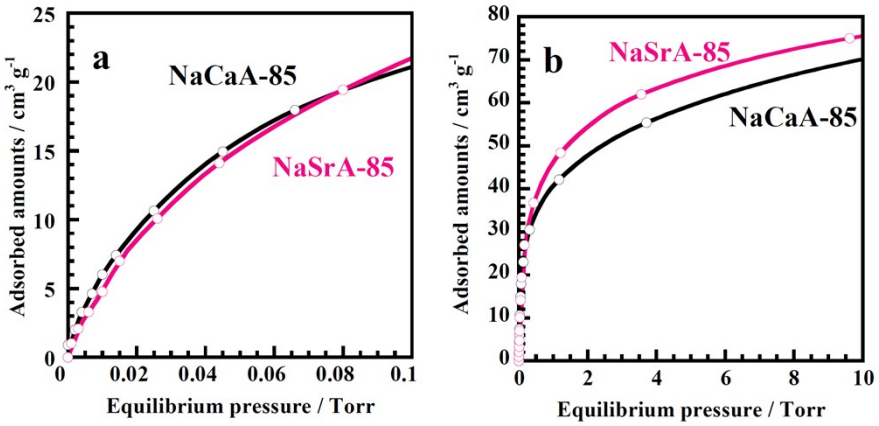

Fig. S5: Comparison of the adsorption isotherms of N_2O on both NaSrA-85 and NaCaA-85 (Isotherms): (a) 0–0.1 Torr and (b) 0–10 Torr.

Fig. S6. S. Hiraki et al.,

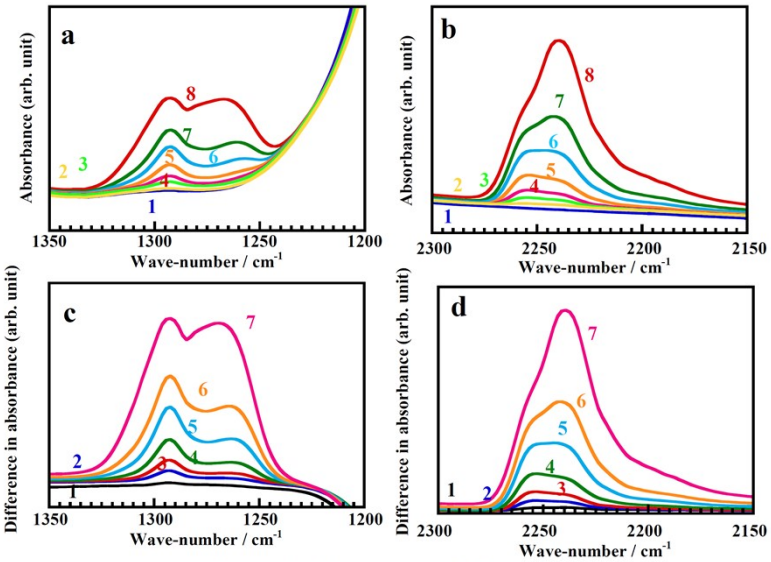

Fig. S6: Mid IR absorption spectra in respective adsorption processes of N_2O on NaSrA-85: (a) ν_1 region and (b) ν_3 region. The sample was (1) evacuated at 723 K, followed by equilibrated with N_2O under various pressures of (2) 0.007 Torr, (3) 0.01 Torr, (4) 0.04 Torr, (5) 1 Torr, (6) 3 Torr, (7) 6 Torr, (8) 21 Torr. The difference spectra between respective adsorption stages and 723 K-evacuated sample: in the (c) ν_1 region and (d) ν_3 region. Difference spectra between spectrum measured under respective pressures and 723 K: (1) 0.007 Torr, (2) 0.01 Torr, (3) 0.04 Torr, (4) 1 Torr, (5) 3 Torr, (6) 6 Torr and (7) 21 Torr.

Fig. S7. S. Hiraki et al.,

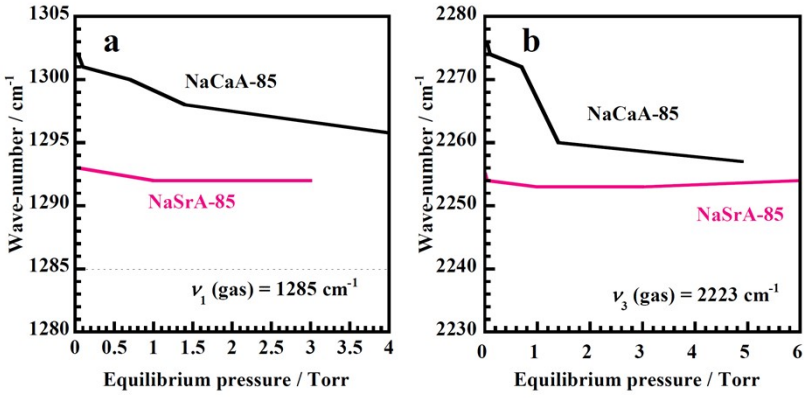

Fig. S7: Plot of change in wave-numbers of N_2O observed in the (a) ν_1 and (b) ν_3 modes as a function of equilibrium pressure.

Fig. S8. S. Hiraki et al.,

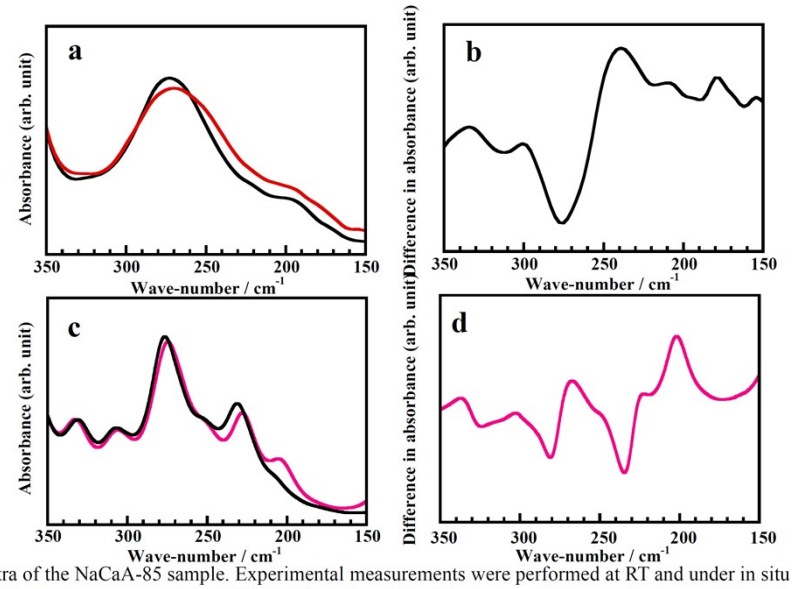

Fig. S8: Far IR absorption spectra of the NaCaA-85 sample. Experimental measurements were performed at RT and under in situ condition. (a) First, the NaCaA-85 sample was evacuated at 723 K: **Black** line. After this treatment, this sample was equilibrated with N_2O under the pressure of 5 Torr: **Red** line. (b) The difference spectrum between them. For comparison, (c) the spectra obtained with the aid of DFT calculation: **Black** line, before N_2O adsorption and **Red** line, after N_2O adsorption. (d) The difference in calculated spectra in Far IR region before and after N_2O adsorption in the NaCaA-85-N_2O system.

Fig. S9. S. Hiraki et al.,

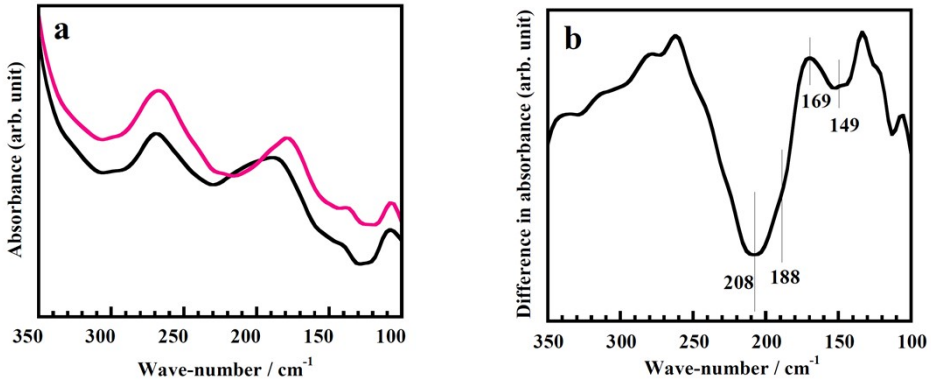

Fig. S9: Far IR absorption spectra and their difference spectrum of the NaSrA-85 sample: (a) before (**Black**) and after (**Red**) N_2O adsorption, and (b) their difference spectrum.

Fig. S10. S. Hiraki et al.,

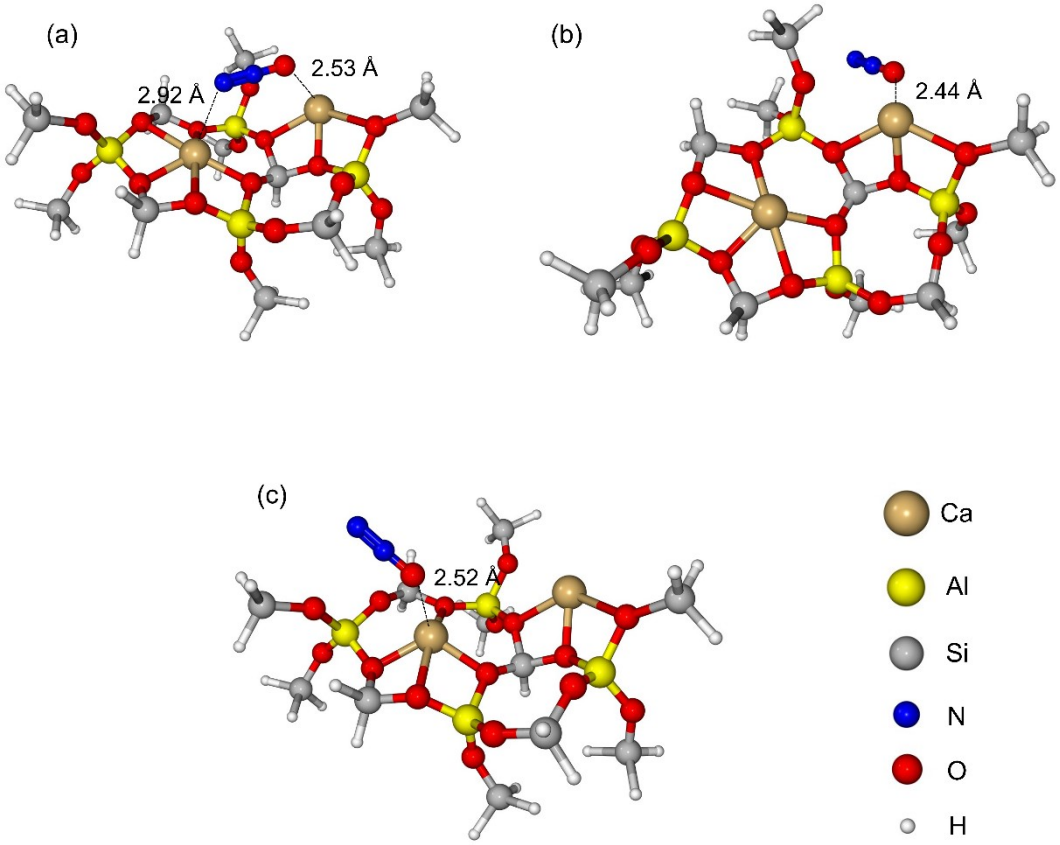

Fig. S10. Resultant optimized geometries of N_2O adsorbed on the respective sites through the DFT calculation: (a) [^{8MR}Ca(N_2O)^{6MR}Ca]-$Al_4Si_{11}O_{16}H_{28}$, (b) [^{8MR}Ca(N_2O), ^{6MR}Ca]-$Al_4Si_{11}O_{16}H_{28}$ and (c) [^{8MR}Ca, ^{6MR}Ca(N_2O)]-$Al_4Si_{11}O_{16}H_{28}$.

Fig. S11a. S. Hiraki et al.,

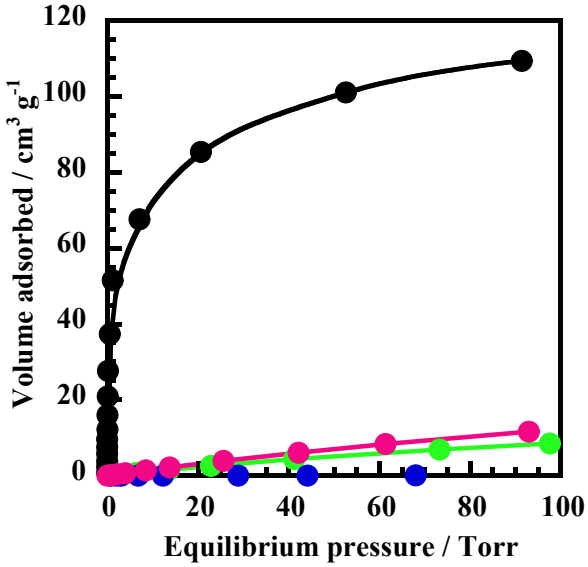

Fig. S11a. Included in this figure for comparison are adsorbed amounts on the NaCaA-85 sample measured at 298 K for various gases; **N_2O** (**Black**), **CH_4** (**Red**), **N_2** (**Green**) and **O_2** (**Blue**), respectively.

Fig. S11b. S. Hiraki et al.,

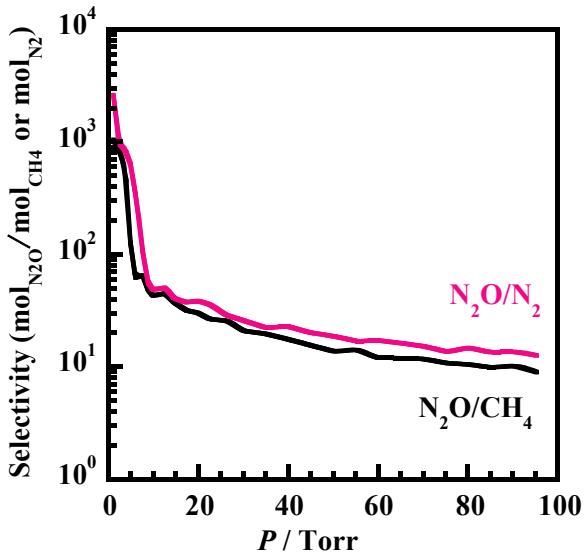

Fig. S11b. Plots of **N_2O/N_2** and **N_2O/CH_4 selectivity** against equilibrium pressures utilizing the NaCaA-85 sample.

Tab. S1a. S. Hiraki et al.,

Table SI-1a: Physical parameters of the vapour adsorbates

Molecule	Kinetic diameter / Å	Polarizability / 10^{-25} cm^3	Dipole moment / 10^{-18} esu cm	Quadrupole moment 10^{-26} esu cm^2
N_2O	3.30	30.3	0.16083	—
CO_2	3.3 —3.9	29.11	0	4.30
CH_4	3.785	25.93	0	0
N_2	3.64—3.80	17.403	0	1.52
O_2	3.467	15.812	0	0.39
H_2	2.827—2.89	8.042	0	0.662
CO	3.690	19.5	0.1098	2.50
NO	3.492	17.0	0.15872	—
H_2O	2.641	14.5	1.8546	—

J.-R. Li, R. J. Kuppler and H.-C. Zhou, Selective gas adsorption and separation in metal-organic frameworks. Chem. Soc. Rev., 2009, 38, 1477–1504.

Tab. S1b. S. Hiraki et al.,

Table SI-1b: Fundamental data of cations.

Molecule	Polarizability / 10^{-25} cm^3	Ionic Radius of Cation / pm	Polarizing Power of Cation (Q/r^2) / 10^{-24} C m^{-2}
Na^+	1.8	12	15.4
Mg^{2+}	0.72	72	61.8
Ca^{2+}	4.71	100	32.0
Sr^{2+}	8.63	118	19.6
Ba^{2+}	15.6	135	17.6

V. Dimitrov, T. Komatsu, J. Solid State Chem. 2012, 196, 574-578.

References in SI section

1. B. Yue, X. Lian, S. Liu, G. Wu, J. Xu and L. Li, Efficient nitrous oxide capture by cationic forms of FAU and CHA zeolites, *Chem. Eng. J.*, 2023, **462**, 142300. This paper is same as the reference 16 in the text.

2. A. Itadani, A. Oda, H. Torigoe, T. Ohkubo, M. Sato, H. Kobayashi and Y. Kuroda, Material Exhibiting Efficient CO_2 Adsorption at Room Temperature for Concentrations Lower Than 1000 ppm: Elucidation of the State of Barium-Ion Exchanged in an MFI-Type Zeolite. *ACS Appl. Mater. Interfaces*, 2016, **8**, 8821–8833.

3. M. Palomino et al., Zeolite Rho: a highly selective adsorbent for CO_2/CH_4 separation induced by a structural phase modification. *Chem Commun.*, 2012, **48**, 215-217.

4. Y. Kuroda, H. Maeda and T. Morimoto, *In situ* sample cell for EXAFS measurements on materials treated at elevated temperatures in vacuo. *Rev. Sci. Instrum.*, 1989, **60**, 3083–3085.

5. Y. Ikemoto, T. Moriwaki, T. Nakano and Y. Nozue, Far infrared microspectroscopy of zeolite MOR single crystal. *Infrared Phys. Techn.*, 2006, **49**, 78–81.

6. A. Oda, S. Hiraki, E. Harada, I. Kobayashi, T. Ohkubo, Y. Ikemoto, T. Moriwaki and Y. Kuroda, Unprecedented CO_2 adsorption behavior by 5A-type zeolite discovered in lower pressure region and at 300 K. *J. Mater. Chem. A*, 2021, **9**, 7531–7545. This paper is same as the reference 6 in the text.

7. S. Grimme, J. Antony, S. Ehrlich and H. Krieg, *J. Chem. Phys*., 2010, **132**, 154104.

8. A. L. Kustov and L. M. Kustov, IR-Spectroscopic Study of Complex Formation of Nitrogen Oxides (NO, N_2O) with Cationic Forms of Zeolites and the Reactivity of Adsorbed Species in CO and CH_4 Oxidation, *Molecules*, 2022, **27**, 55. This paper is same as the reference 19 in the text.